Renewable and Sustainable Energy Reviews 14 (2010) 265–276

Contents lists available at ScienceDirect

Renewable and Sustainable Energy Reviews

journal homepage: www.elsevier.com/locate/rser

Review of study on solid particle solar receivers

Taide Tan, Yitung Chen *

Department of Mechanical Engineering, University of Nevada, Las Vegas, 4505 Maryland Pkwy, Las Vegas, NV 89154, USA

ARTICLE INFO

Article history:
Received 7 January 2009
Accepted 29 May 2009

Keywords:
Review
Solar
Receiver
Solid particle
Water-splitting
Thermo-chemical

ABSTRACT

The solid particle solar receiver (SPSR) is a direct absorption central receiver that uses solid particles enclosed in a cavity to absorb concentrated solar radiation. The SPSR is a candidate for applications of solar energy in a thermo-chemical water-splitting process to produce hydrogen. This paper presents a review of the study on SPSRs, including the idea originality, design concepts, advantages and disadvantages, the solid particle identification, a conceptual design in Sandia National Laboratories and detailed studies performed on this design. The geometry, particle size, calculating domain selection, the wind effect, the aerowindow and other factors which influence the cavity efficiency have been studied and the results are presented.

Contents

1. Introduction

The study on solid particle solar receivers (SPSR) has been years an important research topic for the developing of renewable

* Corresponding author. Tel.: +1 702 8951922; fax: +1 702 8954922.
E-mail address: uuchen@nscee.edu (Y. Chen).

1364-0321/$ – see front matter © 2009 Elsevier Ltd. All rights reserved.
doi:10.1016/j.rser.2009.05.012

Nomenclature

C_D	drag coefficient
d_p	particle diameter
$I(\vec{r}, \vec{s'})$	total intensity
$I_{b,\lambda}$	black body intensity
n	refractive index
Nu	Nusselt number
Pr	Prandtl number of gas flow
$\vec{r}$	position vector
Re_p	relative particle Reynolds number
$\vec{s}$	direction vector
u_j	velocity of air flow (m/s)
U_j	mean velocity of air flow (m/s)
u'_j	fluctuant velocity of air flow (m/s)
$u_{p,i}$	particle velocity
T	temperature
$\bar{T}$	mean temperature
X,Y,Z	coordinates

Greek symbols

α	thermal conductivity
α_λ	spectral absorption coefficient
ε_p	particle emissivity
λ	wavelength
μ	viscosity
μ_t	turbulent viscosity
ν	kinematic viscosity
ρ	density
ρ_p	density of particle
σ	Stefan-Boltzmann constant
σ_s	scattering coefficient

energy systems. The idea originality of an SPSR is to design an efficient receiver as an important part in a water-splitting (WS) thermo-chemical (TC) process to produce hydrogen, which is a promising energy carrier for the future energy supplies. An SPSR is a direct absorption central receiver that uses solid particles enclosed in a cavity to absorb concentrated solar radiation. An SPSR is an ideal candidate for applications of solar energy including fuels and chemicals production, Brayton cycle electricity generation, or industrial process heat applications. The solid particles are heated in an SPSR and serve as a heat transfer and storage medium or as a substrate on which chemical reaction may be performed directly in solar WSTC processes.

This paper presents a review of the study on SPSRs, including the idea originality, the experimental work and numerical studies, and the milestones achievements. Furthermore, the detailed studies of a US DOE funded project on a conceptual design of an SPSR have been reviewed, which is a part of the Solar Thermo-Chemical Hydrogen (STCH) project based on the cooperation of Sandia National Laboratories (SNL) and University of Nevada, Las Vegas (UNLV) [1]. The review will include the conceptual design of an SPSR in the STCH project, the geometry, the particle properties, the calculating domain selection, the wind effect, the protection of an aerowindow and other factors which influence the cavity efficiency. The physical model and mathematical models are analyzed and the solution schemes are presented with the parametric study on different operating conditions and model parameters [2].

2. Hydrogen as an energy carrier

The drawbacks to the fossil fuel use include limited reserves, and carbon dioxide emissions, which is a greenhouse gas responsible for the global warming and environmental pollutions. Hydrogen is a promising and clean energy carrier, which could potentially replace the use of fossil fuels in the transportation sector in the future. The US president George W. Bush's Hydrogen Fuel Initiative [3], announced in 2003, envisions the transformation of the nation's transportation fleet from a near total reliance on petroleum based products to steadily increasing use of clean-burning hydrogen. America's energy security can be dramatically improved with the promising hydrogen projects by significantly reducing the reliance on imported oil, as well as reducing greenhouse gas emissions and helping to clean the air.

Life cycles assessment (LCA) of hydrogen production was first considered by Koroneos in Ref. [4]. LCA is a powerful tool to help evaluate the impact from a process or from production and use of a product. It consists of goal definition and scoping which defines the product, process or activity; inventory analysis which identifies material usage and environmental releases; impact analysis which assesses the human and ecological effects of energy, water and material usage; and last interpretation, which evaluates the results of each analysis. Hydrogen production methods have been compared among natural gas, renewable energy, electrolysis, and fuel in the research. The use of wind, hydropower, and solar thermal energy were proved to be the most environmentally friendly and efficient methods [4].

Hydrogen has much more advantages, as a promising future energy carrier, particularly when coupled with fuel cells. However, there is no environmentally attractive, large-scale, low-cost, and high-efficiency hydrogen production process available for commercialization currently [5]. Hydrogen can be manufactured from a range of energy sources such as fossil fuels, biofuels, renewable energy, nuclear energy via electricity [6–8]. Hydrogen can also readily be produced from synthesized hydrogen carriers such as methanol, ammonia and synfuels. The hydrogen production is mainly based on fossil fuels and most specifically on natural gas at present [4]. There are no environmental benefits if the hydrogen is derived from natural gas or fossil fuel reforming, because of the emissions of CO_2 from these production routes. In addition, hydrogen produced from fossil fuel contains trace contaminants (CO) that are poisons for catalysts used in PEM fuel cells electrodes [1]. A detailed review of the renewably driven hydrogen systems and the modeling approaches have been presented by Deshmukh [7]. The use of wind, hydropower and solar thermal energy for the production of hydrogen are the most environmental friendly methods. Among which, the WSTC cycle is one of the most promising methods to produce hydrogen, especially when it is driven by solar energy.

3. Solar-driven water-splitting thermo-chemical (WSTC) cycles for hydrogen producing

Electrolysis produces pure hydrogen but suffers from thermodynamics inefficiencies. The projected efficiency for the electrolytic path is about 36%. However, the current combined efficiency does not exceed 20–25%. The overall efficiencies of the most investigated WSTC cycles are in the range of 45–50% [1,5]. Therefore, a WSTC cycle is one of the most promising methods to produce hydrogen from the point view of efficiency. In a WSTC cycle, water and heat are the inputs, and hydrogen and oxygen are the only outputs. The other chemical and reagents are recycled in a closed WSTC.

As the opposite beneficial aspect of the oil crisis, the interest in WSTC processes boomed in the late 1970s and early 1980s [9–11].

The researches in WSTC then slowed down worldwide till the last review published in 1989 [11]. Some continuing work has been carried out, but mostly in those countries where the dependence upon foreign energy sources is of the national concern, such as Japan. Several hundred WSTC processes have been proposed for the hydrogen production. However, the technical feasibility study and efficiency evaluation have been executed on only a few of these cycles [5].

Typically, a WSTC process to produce hydrogen requires a heat input in excess of 700 °C. This heat can be either supplied by solar or by nuclear energy. Historically, processes receiving the most attention were those having a maximum temperature of around 900 °C that could be linked with a nuclear energy input. The TC processes evaluation and screening were generally conducted in the frame of the coupling with an advanced high-temperature nuclear reactor as the primary energy source [9–11]. Thus, the maximum cycle temperature level was the deemed optimum for an advanced high-temperature nuclear reactor, i.e. about 850 °C. Hence, the range selected for the optimum maximum temperature in process was 750–850 °C [12]. The Adiabatic UT-3 cycle was proposed at the University of Tokyo [13,14] and selected by JAERI for further development. The predicted efficiency of the Adiabatic UT-3 process varies between 35% and 50% depending upon the efficiency of membrane separators, which are under development, and also depending on whether electricity is co-generated along with the hydrogen. The UT-3 cycle is based on two pairs of chemical reactions. The first two ensure the formation of hydrobromic acid releasing oxygen, and the other two ensure the reduction of water by a bromide. The maximum temperature of this cycle is about 742 °C [15], which can be driven by either the nuclear energy [13,14] or the solar energy [16–19].

The Sulfur-Iodine (SI) cycle was developed by General Atomics [14]. The SI cycle [20] remains the cycle with the highest reported efficiency, theoretically 52%, based on an integrated flow-sheet with suggested process improvements that could increase the efficiency and lower the capital cost [21]. The SI cycle has a maximum reaction temperature of 850 °C [22]. Therefore, the primary energy input has been designed originally to be supplied from the advanced nuclear power station (4th generation) [23,24]. The hybrid sulfur (Hy-S) processes, proposed by Westinghouse [25], is another typical cycle of the hydrogen production process, having a same maximum temperature as an S-I cycle [26]. The Hy-S cycle is a variant of the sulfur-iodine cycle and it involves a thermochemical and an electrochemical reaction. Actually, the energy for SI cycle and the Hy-S cycle can be supplied by both solar energy and nuclear energy from their maximum temperature requirements.

The solar energy is obviously a much "cleaner" energy compared to the nuclear energy as an energy input for the WSTC process. Moreover, many of the TC reactions require a minimum of over 1000 °C or even higher than 2000 °C, such as the Zinc-Oxide cycle [27]. These kinds of TC cycles are considered as solar energy only in a temperature higher than 1000 °C is required. Therefore, WSTC cycles may constitute the optimized choice for hydrogen production [28].

Viable water splitting cycles have been identified and evaluated basically at a high temperature, which can be driven by solar energy and can offer potential for efficient and large-scale production of hydrogen [5]. Studies about two-step cycles at a high temperatures were related to CdO/Cd (1400 °C) [29], ZnO/Zn (2000 °C) [30–32], Fe_3O_4/FeO (2200 °C) [33–36] initially proposed by Nakamura [37]. The use of mixed metal oxides (e.g. zinc–ferrite, manganese–ferrite, or nickel–ferrite) cycles decreases the temperature of the activation step while the reduced oxide remains reactive for the H_2 generation step [38–46]. A project funded by the DOE was initiated in the USA recently. This project aims at identifying and testing the high-temperature solar-driven TC cycles [47]. A computer searchable database including 280 cycles [48] was developed as the tool to organize the cycle data. The feasibility of the main part of the cycles has not been proved yet and only a few were tested experimentally. The basic screening and testing work on the promising solar-driven WSTC cycles can be found from Refs [5,49].

4. Central receivers for WSTC cycles

Solar energy is much more environmentally and technically acceptable as a heat source for a WSTC process, especially at a high temperature. However, solar thermal energy must be collected by concentrated methods in order to achieve reasonable temperatures in a working medium.

The prevailing wisdom with regard to the design of WSTC hydrogen production facilities is that bigger is better due to the economies of scale and operational considerations. Therefore, the preference of the WSTC processes will be those which are suitable for a central receiver platform [50]. A central receiver facility has the potential to offer thermal storage and "around-the-clock" operation. Concentrated solar energy can be collected by a solar central receiver system which uses a field of heliostats to reflect and focus sunlight onto a receiver located on top of a solar tower [2]. In this manner, the collected sunlight can reach hundreds of suns at the surface of the solar receiver. The concentrated solar energy is capable of attaining the temperature requirement for the TC reaction cycle at 2000 °C or even higher. The principal challenges for central solar receivers in a WSTC process include the selection a suitable work media for heat transfer and storage and the design and efficiency improvement of a solar receiver. A working medium is needed to transport the energy for the reactions that need heat source. Previous studies on the working medium in a solar central receiver have been on gases or liquids which need to be transported by tubes or pipes. There are working demonstrations of systems using liquid as the heat medium like the water/steam central receiver system, located near Barstow, California, which produces electrical energy [51]. The other common working fluids are molten salts, molten metals, and air. The term solid particle solar receiver is another concept of a heat energy transfer medium with great interest. Sand-size refractory particles are falling down freely inside a solar receiver to form a curtain that directly absorbs the solar insolation. An SPSR has many favorable characteristics compared to other solar receivers. For example, the solid particles absorb the concentrated solar flux directly and the particles themselves serve as the storage medium in an SPSR [2]. Therefore, a conceptual simplicity can be obtained and a high temperature (above 1000 °C) can be obtained, which is not allowed with other systems, since a fluid conduit and additional piping and heat exchanger equipment are not necessary [52]. Moreover, there are other advantages, such as, the economicity and abundance of possible receiver materials, the possibility of building a simple thermal storage system (a tank filled with the hot particles), the absence of piping and heat exchange problems such as those related to the use of molten salts (freezing problems), air or steam (poor heat transfer). Furthermore, there is no excessive thermal stress on the plant components since the heat is directly absorbed by the particles without heating receiver pipes or cavities.

However, the existing open aperture lowers the overall efficiency by convection heat transfer. It is necessary to minimize heat loss from the particles to the air within the receiver as this lowers the overall efficiency [53]. Apparently, the solid particle receiver addresses both of the two principal challenges of a central receiver.

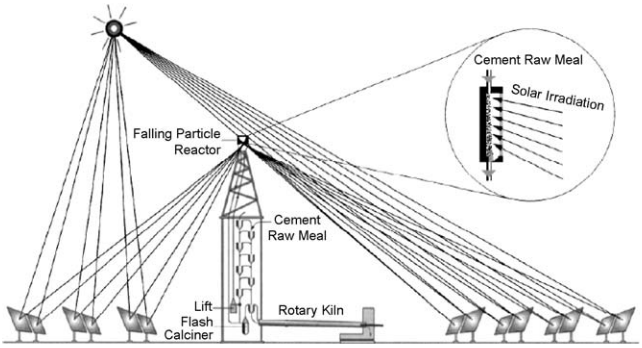


Fig. 1. Simplified schematics of the solar falling particle reactor (FRP) [53].

The simplified schematics of the solar falling particle reactor (FRP) system are shown in Fig. 1 [53]. An SPSR is usually mounted atop a tower to capture the focused solar energy from a field of heliostats. The solid particles are lifted to the top of the SPSR and then fall as a cloud or curtain through the receiver where they are irradiated directly by concentrated sunlight passing through the aperture of the SPSR. The particles are typically dark in color and made of a ceramic material such as sintered bauxite. The heated particles can then be stored and run through a heat exchanger to provide thermal energy input to a process [2].

There are also many other kinds of solar receivers under investigation. In some designs of the central receivers, the heat absorbing and reaction progress occur in the same place [4,26,54,55]. For example, an atmospheric-open cyclone solar receiver–reactor has been designed and tested by Steinfeld to decompose the carbonates and hydroxides of Group IIA elements in the periodic table [56]. The receiver–reactor is tested with the decomposition of calcite which needs a reaction temperature of 1170 K. The energy absorption efficiency, based on the energy incident on the receiver aperture, was 43% [56]. However, this kind of receiver is not suitable for the reactions in which liquid is present, or in which the products is need to be isolated from the oxygen in the atmosphere [56].

5. Research on SPSRs

Initially, the SPSR has been studied in the early 1980s in order to create a direct absorption central receiver which is able to interface with high temperature (>900 °C) electric power and chemical-production cycles [57].

Martin and Vitko studied the falling solid particles, as a pioneering work, in a solar central receiver at SNL [57]. The heat absorption characteristics of particles have been studied using a radiant heat source [52]. Possible particle materials have been evaluated with respect to optical properties and structural stability [58,59]. Some experiments have been made on the dynamics of the particles and on the heat exchange [60–62]. The early work on the research of SPSR has been reviewed and summarized by Falcone [62–64]. More recent SPSR work included on-sun testing and optical characterization of a 2 MWt SPSR prototype capable of achieving a temperature higher than 300 °C at SNL [65].

Computational models have been built to simulate receiver operation and to aid in design efforts [51,64]. Many theoretical simulations have been performed on the internal fluid dynamics of the receivers, in various configurations [53,66–69]. All these studies simulate with global models the radiation absorption of the particle curtain, the thermal transport between the particles, the air and the cavity, and the fluid dynamics of the air in the cavity; these are all fundamental aspects to assess the efficiency and the working temperature of the plant. The particle temperature and the efficiency of energy absorption of the receiver have been investigated by Evans [66–68] utilizing numerical models. Using computational fluid dynamics (CFD) technique, the performance of a solar falling particle reactor in a pilot plant was investigated by Meier [53]. The models, however, were limited to two-dimensional cases due to a limitation in computational resources and most of these models did not consider the interaction between the particles and the flow inside the SPSR. The 3D numerical model was built by Chen [69] and the impact of the particle size and other operating conditions on the performance of the SPSR have been studied numerically. However, the 3D study was confined in the receiver only. In fact, the heat change between the air inside the cavity and the air outside the cavity is rather important, especially when a wind field is present.

Windows for solar receivers are usually expensive, brittle, require careful mounting, but often fail to withstand the high solar fluxes and high temperature, reducing the solar energy absorption efficiency [56]. Aerowindows have the potential of increasing the efficiency of an SPSR by reducing convective losses from an open receiver aperture and eliminating reflection, convection and reradiation losses from a comparable glass window. Aerodynamic windows consist of a transparent gas stream, which is injected from an air jet across the receiver aperture to isolate its interior from the surrounding atmosphere [2,70–74]. Even though, the wind conditions may still have an important effect on the performance of SPSRs. The aerodynamics and thermal interactions between gas flow and solid particles are very complicated due to the combination of convective and radiative exchange. The complexity increases considering the combined influence of the aerowindow flow and the wind [2,72–74]. The wind effect on the performance of an SPSR has been investigated recently, with or without the protection of an aerowindow [2,72–75]. In this present design, the SPSR is only used as a heat absorbing device.

6. Solid particle selection

The technical feasibility study of solid particles has been conducted and concluded by Hurby in SNL [51,52,61,62,64]. The candidate particle materials for a SPSR must have at least three important characteristics: (1) low propensity towards agglomeration, (2) high fracture resistance, and (3) large solar absorptivities. Furthermore, the particles must be inexpensive and readily available in large quantities.

The initial material evaluation studies considered some traditional high temperature ceramic materials available in the particle sizes of interest in SNL [51,52,61,62,64]. Techniques have been established for evaluation the agglomeration, fracture and optical properties characteristics of the SPSR candidate solid materials, from alumina, silica, silicon carbide, zircon, etc. Custom experimental devices for high temperature radiative optical properties measurements have been designed. The agglomeration investigation has indicated that the best behaving pure ceramics for use at 1000–1200 °C are alumina, silica and zircon. Fracture resistance studies have indicated that critical impact velocity can be related to the compressive strength and facture toughness of the particle. It was found that impact-induced fracture is probably not a problem for small rounded ceramic particles in an SPSR. The effect of solar cycling on the compressive strength can be examined by cycling paced particle samples in a solar furnace. Toughness can be examined as a function of static heat treatment. Bulk solar absorptivity measure has indicated that the candidate material which performed the best with respect to agglomeration had low solar absorptivities [51,52,61,62,64]. This indicated that additional materials must be considered in order to find a better solution of the particle selection, which satisfies the physical and economic characteristics, in the further development of SPSRs.

7. Physical model for the numerical simulation of performance evaluation of an SPSR

A conceptual design of a solid particle receiver has been proposed for experiments at SNL, as a part of the STCH project sponsored by the DOE in the U.S. [2,69,72–74]. The working solid particle curtain used in SNL for testing is called CARBO-HSP, a commercial product from CARBO Ceramics, which contains mainly bauxite and about 7% iron oxide. It is assumed that the particles are spherical in shape (sphericity of 0.9). The detailed parametric study has been conducted on this conceptual design and the results will be present in the following sections.

The typical aerodynamic and thermal processes in a SPSR are analyzed and shown in Fig. 2. Solar energy is concentrated and directed to the receiver from the aperture by heliostats on the ground. The solid particles are fed from the top of the receiver. In order to separate the hot hair within the receiver and the cold air out of the receiver, an air jet may be added on the top of the aperture. The aerodynamic behaviors of the particles are impacted by the wind, the air jet flow, the air flow inside the receiver induced by the falling of particles, and the temperature difference. Also, the thermal interactions which include particle–particle radiation, particle-wall radiation, particle-air convection, and air-wall convection, are needed to be investigated [2,72–74].

8. Mathematical model

The air flow inside the solid particle receiver can be influenced by drag forces and buoyant convective heat transfer in the vicinity of the particles because of the interaction with the particles. The particle volume fraction in the SPSR has been found to be less than 0.1% [60,69]. Therefore, the collisions between particles are negligible. Hence, the two-way coupled Euler-Lagrange method, which includes the exchange of heat and momentum between the gas phase and the solid phase, is used to simulate the gas-particle flow in this paper. Particle–particle collisions and the resulting momentum transfer are not included at present.

With the typical operating conditions of the receiver, the characteristic Reynolds numbers within and out of the receiver are calculated to be larger than 1.0×10^5. Therefore, a turbulent flow is expected within and outside of the receiver. The time-averaged governing equations for conservation of gas phase mass, momentum, and energy will be solved [2,69,75].

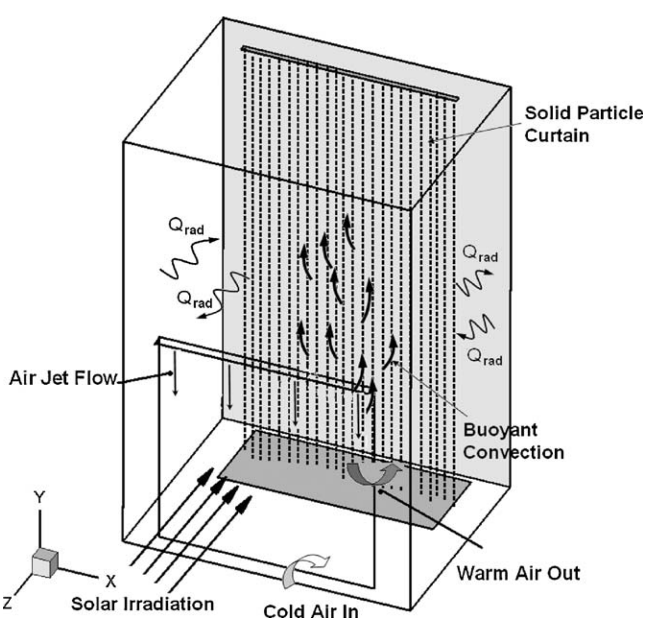


Fig. 2. Typical aerodynamic and thermal processes in a solid particle receiver with air jet flow.

A realizable k–ε model is used for closing the turbulent Navier–Stokes equation system. A bibliographical study concerning the validation of the CFD model, including the turbulence model (the realizable k–ε model), showed that this approach has been extensively validated for a wide range of flows, including the channel and layer flows [2,60,69,75]. Compared with the standard k–ε model, the realizable k–ε model is likely to provide superior performance for flows involving rotation, boundary layers under strong adverse pressure gradients, separation and recirculation (including flows over obstacles). For all of these cases, the performance of this model has been found to be substantially better than that of the other turbulence models. The realizable k–ε model was also proved to be a preferable model for successful 3D simulation of air flow inside the SPSR and interactions of solid particles and the air by Chen [69]. The details of the realizable k–ε model have been given Refs. [2,69,75], together with the differences with the standard k–ε model and the advantages of the realizable k–ε model.

By integrating the force balance on the particle, the trajectory of the particles can be predicted in a Lagragian reference frame. This force balance equates the particle inertia with the forces acting on the particle, and can be written as

$$\frac{du_{p,i}}{dt} = \frac{18\mu}{\rho_p d_p^2}\frac{C_D Re_p}{24}(u_i - u_{p,i}) + \frac{g_i(\rho_p - \rho)}{\rho_p} \tag{1}$$

where the relative Reynolds number Re_p can be calculated by,

$$Re_p = \frac{\rho d_p |u_{p,i} - u|}{\mu} \tag{2}$$

The suitable empirical equation for the drag coefficient for the particles in the solar receiver is proposed by Clift [76],

$$C_D = \frac{24}{Re_p}(1 + 0.15 Re_p^{2/3}) \tag{3}$$

The effect of the pressure gradient and particle acceleration on drag coefficient can be neglected since the material density ratio between particle and air is larger than 10^3. The energy equation for the particle is given by

$$\frac{\rho_P c_p \pi d_p^3}{6}\frac{dT_p}{dt} = Nu\lambda\pi d_p(T - T_p) + \pi d^2 \varepsilon_p \sigma(T_R^4 - T_p^4) \tag{4}$$

In order to predict the interaction of an incident radiation field with the falling particle curtain and receiver wall accurately, the discrete ordinate method with a solar ray tracing model is used to calculate the radiation field inside the receiver. The radiative transfer governing equation for the spectral intensity $I_\lambda(\vec{r}, \vec{s}')$ of an absorbing, emitting, and scattering medium, at position $\vec{r}$ in the direction $\vec{s}$ can be written as [69,75],

$$\nabla \cdot (I_\lambda(\vec{r}, \vec{s})\vec{s}) + (a_\lambda + \sigma_s) I_\lambda(\vec{r}, \vec{s}) = a_\lambda n^2 I_{b\lambda} + \frac{\sigma_s}{4\pi}\int_0^{4\pi} I_\lambda(\vec{r}, \vec{s}')\Phi(\vec{s}, \vec{s}')\, d\Omega \tag{5}$$

The radiative transfer equation is solved for a finite number of discrete solid angles, each associated with the vector direction $\vec{s}$ fixed in the Cartesian system (X, Y, Z) in the discrete ordinates radiation model. The discrete model transforms the radiative equation into a transport equation for radiation intensity in spatial coordinates. The solar ray tracing algorithm is employed to predict the direct solar illumination energy source that results from incident solar radiation [69,75]. This algorithm takes a beam that is modeled using the sun position vector and illumination parameters, applies it to any or all wall or inlet/outlet boundary zones specified, performs a face-by-face shading analysis to determine

well-defined shadows on all boundary faces and interior walls, and computes the heat flux on the boundary faces that results from the incident radiation [75].

9. Numerical procedure

The above governing equations are solved in the Cartesian coordinate system with a control-volume finite difference method. A non-staggered grid storage scheme is adapted to define the discrete control volumes. A power law differencing scheme is employed in the present paper and the solver used is a segregated solver. In order to resolve the coupling between pressure and velocity, the SIMPLE algorithm is adopted. The governing equations, which were discrete and non-linear, are linearized using an implicit technique with respect to set of dependent variables. The algebraic equations are solved iteratively using an additive correction multi grid method with a Gauss-Seidel relaxation procedure.

9.1. Wind speed classification and wind attacking direction

The wind speed classification based on Beaufort-values is used in the present investigation [77,78]. The wind speed range from "light air" to "fresh breeze" (Beaufort number 1–5) will be studied. With each Beaufort number, a typical speed is employed for the present model. The typical values and the wind speed classification are listed and analyzed in Ref. [2]. The statistics of wind speed from a local station in Las Vegas, Nevada, U.S. [79] are illustrated in Fig. 3. From Fig. 3, the selected wind speeds for studying (from Class 1 to 6) are ensured to cover most of the wind speeds in the local region [2].

Fig. 4 shows an SPSR in a wind field with an attacking angle. Two kinds of wind fields will be investigated. The first kind of wind filed is wind blowing parallel to the ground. The attacking angle α (in plane of XOZ), from the top view of the domain, stands for the angle between the wind velocity and the normal vector of the aperture. The typical wind directions studied in the present model are $\alpha = 0^\circ$, $\alpha = 45^\circ$, and $\alpha = 90^\circ$. Assuming the aperture is facing the south direction, the wind is attacking from the southwest direction in the cases of $\alpha = 45^\circ$. The results with wind attacking from the southeast direction ($\alpha = 135^\circ$) are assumed to be the symmetrical to the results of $\alpha = 45^\circ$. In the case with $\alpha = 0^\circ$ the wind attacking direction is normal to the aperture. While, wind blows tangential to the aperture in the cases of $\alpha = 90^\circ$. The attacking angle β (in plane of YOZ in Fig. 4) is used to distinguish the different angle of wind from the side view of the domain. An attacking angle of $\beta = 90^\circ$ stands for wind blowing from the top and $\beta = -90^\circ$ stands for wind blowing from the bottom, both tangentially to the aperture. An attacking angle of $\beta = 45^\circ$ stands for wind blowing from the top but with an angel of 45° and $\beta = -45^\circ$ stands for wind blowing from the bottom and with an angel of 45° to the vector of the aperture.

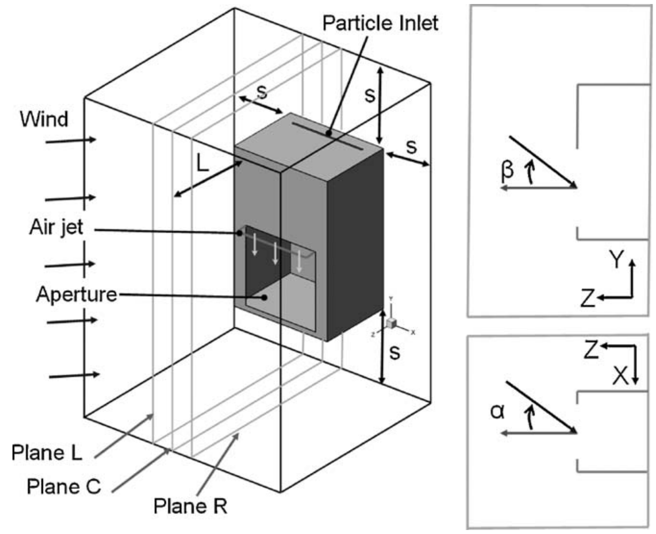


Fig. 4. The domain for CFD simulation of the wind effect on the solid particle receiver.

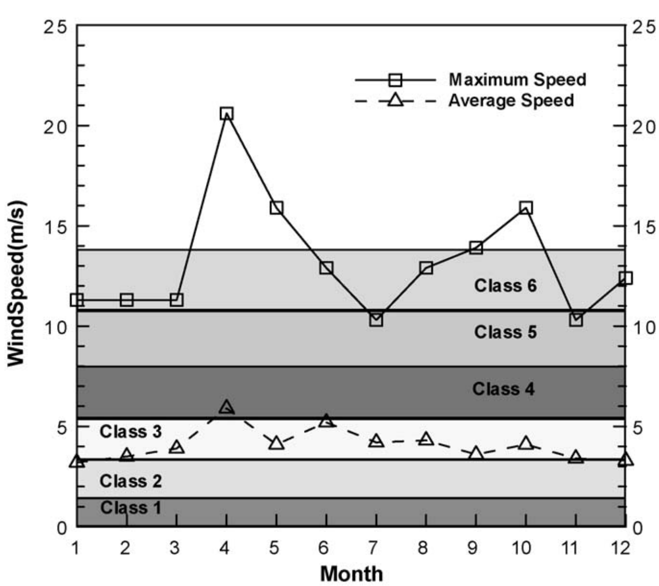


Fig. 3. The statistics of wind speed in Las Vegas and the typical values for study in the present model.

9.2. Selection of solar incident radiation flux

The statistics of solar incident radiation from a local station in Las Vegas, Nevada, U.S. [78]. The eight hours average values (from 8:00 to 16:00) and the ten hours average values (from 7:00 to 17:00) are calculated and plotted in Fig. 5. Typically, a uniform solar incident radiation flux of 920 kW/m^2 is employed for the solar receiver performance calculations [66,68,69]. In order to provide this amount of solar radiation flux, 1195 solar heliostats

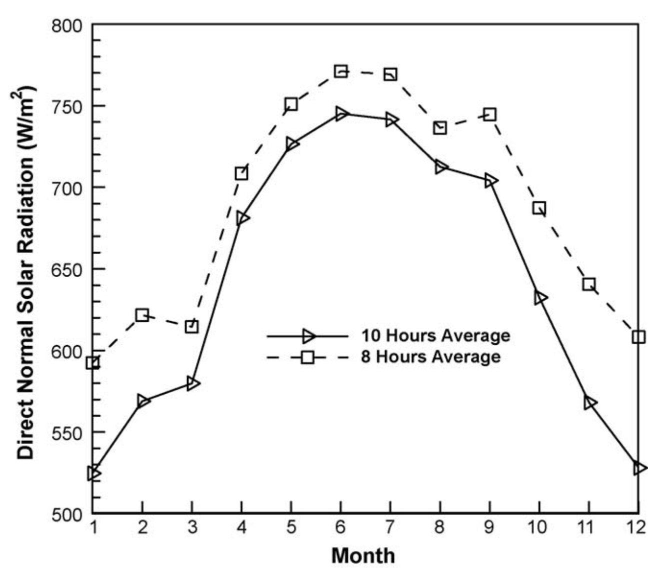


Fig. 5. The average solar incident radiation in Las Vegas.

units are needed for the maximum values of solar radiation (in June and July), whereas 1559 solar heliostats units are needed for the minimum values of solar radiation (in January) based on the eight hours average value. If ten hours operating time is required, 1260 units and 1769 units are needed for the maximum and minimum values of solar radiation in order to provide solar incident radiation flux of 920,920 kW/m^2 [2].

9.3. Geometry

Different designs of the SPSR have been proposed in SNL. For example, a commercial design with 5 m wide, 4 m deep and 6.7 m high has been proposed [70]. However, the experimental and numerical data for this commercial size receiver is still sparse. Another simple designer for the distribution of the particles after dropping has been set up in SNL [70]. In this simple design, there is no top board and front board and the size is 0.4 m $\times$ 0.4 m $\times$3 m. The solar radiation energy is not load on the particles and the thermal aspects have not been taken into accounted. Another conceptual design of the SPSR in SNL for laboratory testing and numerical investigation is shown in Fig. 6, including the schematic geometry and dimensions. The geometry of this conceptual design consists of a three dimensional rectangular cavity that is 2 m wide, 1.58 m deep and 3 m high. The width of square aperture which allows for the incident solar flux is 1.5 m. An opening of 0.25 m by 1.5 m at the top is used for the introduction of particles. The heated solid particles will be storage in the catch hopper for the high temperature solids storage after falling through the receiver from the top inlet. The parametric study will be conducted with this conceptual design.

9.4. Calculating domain selection

The research of wind effects on an object is an important subject because of its technological significance, such as for a skyscraper or

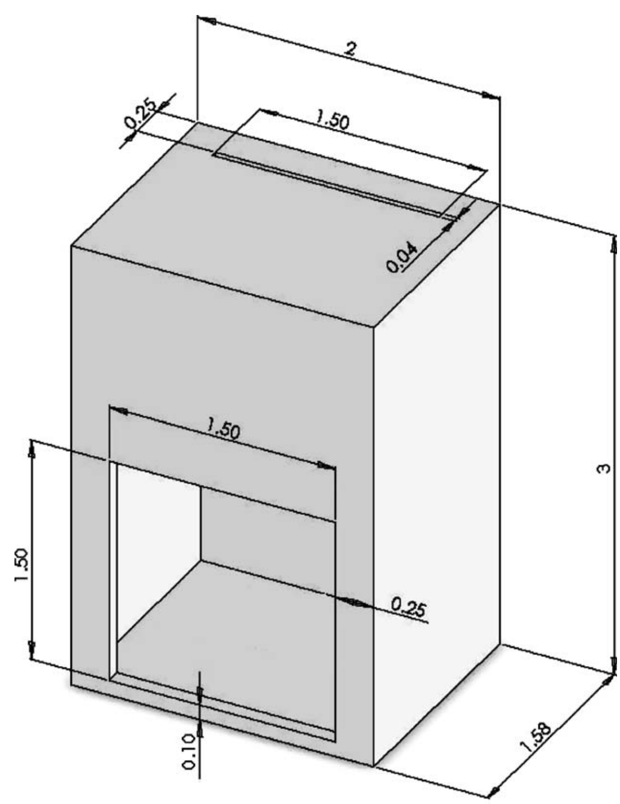


Fig. 6. A schematic geometry of a solid particle receiver (unit: m).

a bridge in a strong wind field. However, most of the researchers selected a much larger domain than the object for studying. The dimensions of the calculated domains are chosen randomly, as long they are assumed large enough [80–83]. For the present 3D numerical model considering the wind effect, the mesh for calculation should be refined in the receiver, and should be even finer in the region close to the particle curtain. The mesh for the wind field can be coarser. In order to make the mesh system smoother and to save the calculating time, the calculating domain is better to be as small as possible as long it can capture the main phenomena in the receiver. Therefore, a domain independent study is necessary. To simplify the domain independent study, the space dimensions for each side (up, down, left and right) will employ a same value, S, while the approaching length is assumed to be *L*, as shown in Fig. 2. During the domain independent study, the approaching length 3 m, 5 m, 7 m, 10 m, and 15 m are studied. Later on, the side space is studied for $S = 0$ m (without side space), 1 m, 3 m, 5 m, 7 m, and 10 m. As reported in Ref. [2], the approaching length $L = 7$ m and side space $S = 3$ m can be considered a good choice for calculation since both the pressure and velocity difference are less than 5% with more increase of the size of the calculating domain [2].

9.5. Mesh independent study

After determination of the calculating domain, the grid independence is checked. Four mesh systems have been created for numerical simulation. Mesh #1 has 222,939 nodes and 209,320 hexahedral cells; mesh #2 has 597,350 nodes and 624,120 hexahedral cells; mesh #3 has 1,068,926 nodes and 1,031,076 hexahedral cells; mesh #4 has 1,563,626 nodes and 1,501,236 hexahedral cells. The differences for both values decrease to less than 5% when the mesh nodes increases to 1,068,926 (mesh #3). To save the calculating time and to ensure the accuracy, a mesh with 1,068,926 nodes and 1,031,076 hexahedral cells (mesh 3) is selected for the present work [2,72].

10. Numerical results and discussions

A two band isotropic radiation calculation is made with a solar band from 0.2 to 1.5 μm and an infrared band from 1.5 to 30 μm. etailed information related to the input conditions of the analysis and the physical properties of the solid particle are given in Table 1. Diffusely scattering bounding walls with an emissivity of 0.8 are used. It is assumed that the walls are perfectly insulated to be adiabatic.

10.1. The particle size influence

A smaller size of the particles leads to a higher cavity with the same operating conditions. This conclusion has been demonstrated in Ref. [69] with consideration with or without the outlet opening at the bottom of the receiver. Chen [69] studied different size of solid particles from 200 to 1000 μm and the cavity efficiency keeps

Table 1
Simulation conditions and solid particle properties.

Gas flow	Solid particle
Operating pressure: 101,000 Pa	Particle density: 3200 kg/m^3
Air outlet condition: pressure outlet	Heat capacity: 1085 J/kg K
Wind temperature: 300 K	Thermal conductivity: 6.67 W/m K
Air jet temperature: 300 K	Particle emissivity: 0.9
Back flow temperature: 300 K	Particle diameter: 650 μm
	Particle total flow rate: 5.0 kg/s
	Particle initial temperature: 873 K
	Particle initial velocity: 0.088 m/s

dropping. The same conclusion has been drawn by Chen [84] in her simulation with consideration of cooling effect of the atmosphere. However, the solid particle size selection should take into account the manufacturing issues and a too small size of the particle may cause the escape of the particles from the aperture. Obviously, the particle distribution at the exiting opening is impacted by the particle size.

10.2. The influence of the bottom opening

The heated solid particle will be released form the bottom of the receiver. One scheme is to keep the exit open all the time and another scheme is to keep the exit close and only open it after collecting a stack of particles. In the case of the receiver with a bottom opening, the hot air exits with the particle flow through the bottom of the receiver when the outlet opening is open. In the case where particles are allowed to exit the bottom of the receiver the average receiver temperature is lower than the averaged receiver temperature in the case where the particles are not allowed to exit, due to the increased backflow of air from the aperture [69]. Therefore, a case with bottom opening has lower cavity efficiency than a case with a closed bottom opening.

10.3. The wind effect without protection of an aerowindow

The cases with different wind speed and attacking direction has been examined without the aerowindow protection. At first, the cases with different wind speed and attacking normal to the aperture ($\alpha = 0^\circ$, $\beta = 0^\circ$) is examined without the aerowindow protection. Then, the wind attacking direction effect on the performance of a solid particle solar receiver has been studied with different angle of α and different wind speeds. When the angle α is studied, the angle β is kept to be zero in all the cases.

Fig. 7 shows the cavity efficiency for each case, and Fig. 8 shows the particle exiting temperature for all the cases. The results are compared with results from the cases with normal wind velocity ($\alpha = 0^\circ$). From Fig. 8, the solid particles can be heated up to 1050 K or a higher temperature successfully with this small conceptual experimental design. An SPSR in a field without wind undergoes large convection loss and has very low cavity efficiency without protection of an aerowindow. When wind attacks normally to the aperture, a stronger wind blowing normal to the aperture will keep more hot air in the cavity so that higher cavity efficiency can be obtained. The cavity efficiency of the cases with wind an attacking angle $\alpha = 45^\circ$ has no significant difference from the cases with normal wind attacking. The wind with a low velocity can reduce the large convective heat loss so the SPSR has slightly higher cavity efficiency than the normal wind cases. With a high wind speed (larger than 4.5 m/s), the wind with an attacking angle $\alpha = 45^\circ$ causes strong turbulence in the cavity and results in a lower cavity efficiency than the cases with $\alpha = 0^\circ$. The efficiency and the particle exiting temperature of the cases with wind an attacking angle $\alpha = 90^\circ$ keep the same tendency with the cases with the cases of $\alpha = 45^\circ$ and $\alpha = 0^\circ$. Basically, the cavity efficiency tends to increase when wind spend increases.

Then, the wind effect of different attacking angle β is studied, while the angle α is kept to be zero. The cavity efficiency of cases in which wind blows from the top (with positive β, typically $\beta = 90^\circ$ and $\beta = 45^\circ$) is shown in Fig. 9, compared with the cases in which the wind blows normal to the aperture. The efficiency of an SPSR in a wind filed with $\beta = 45^\circ$ increases greatly when wind velocity

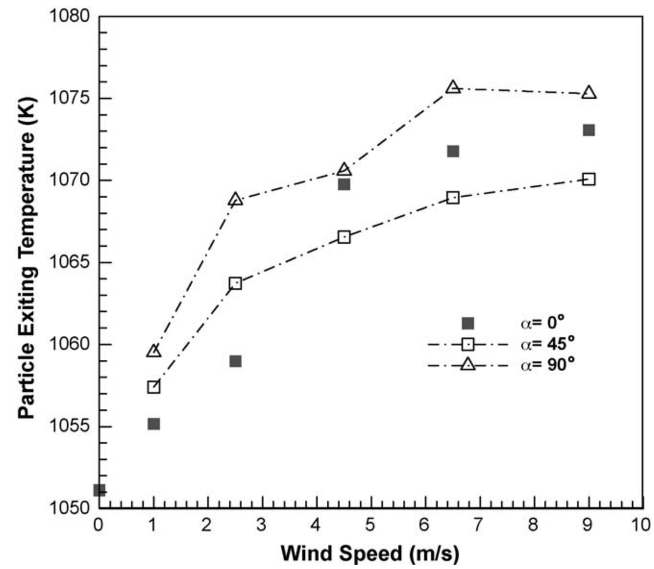


Fig. 8. The cavity efficiency for different wind speed and attacking angle α ($\beta = 0^\circ$).

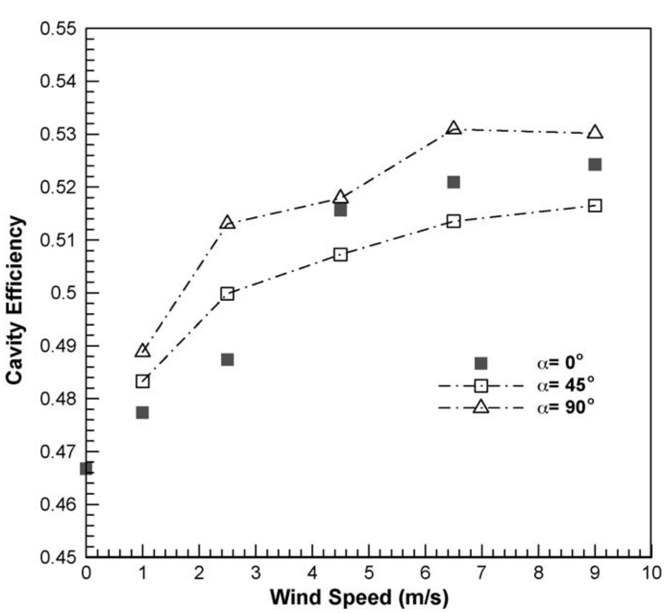


Fig. 7. The cavity efficiency for different wind speed and attacking angle α ($\beta = 0^\circ$).

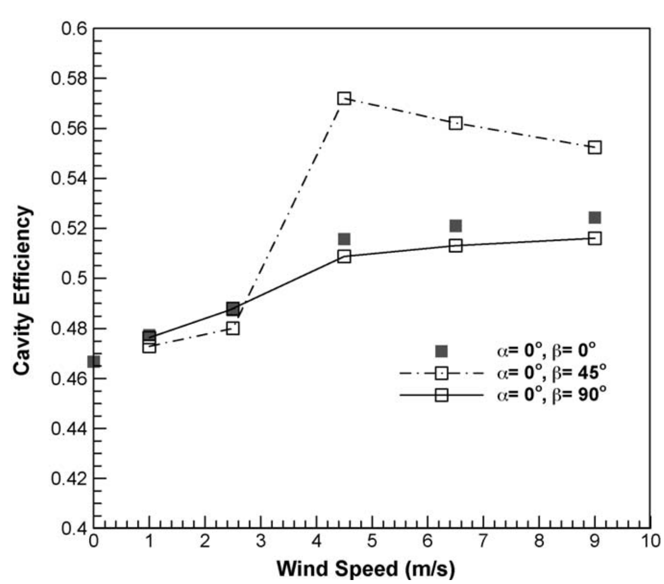


Fig. 9. The cavity efficiency for different wind speed and attacking direction (with $\alpha = 0^\circ$ and positive β).

increases from V_{wind} = 2.5 m/s to V_{wind} = 4.5 m/s and then drops slowly because the blowing wind can not prevent the large loss of the heated air from the aperture at a low wind velocity. However, the blowing wind serves as an new "aerowindow" and keeps most of the hot air in the cavity, when the wind velocity reaches 4.5 m/s or higher. On the other hand, a higher wind velocity will bring more cold air into the cavity and the cavity efficiency starts to drop again after the wind formed "aerowindow". The cavity efficiency of the cases with $\beta = 90^\circ$ is relatively low and has no obvious difference with the cases with $\beta = 0^\circ$.

The cavity efficiency of cases in which wind blows from the bottom (with positive β, typically $\beta = -90^\circ$ and $\beta = 45^\circ$) is shown in Fig. 10, compared with the case in which the wind blows normal to the aperture. From the comparison, the wind effect on the cavity efficiency is more complex when wind blows from the bottom. For an SPSR in wind filed with $\beta = 90^\circ$, the cavity efficiency increases with wind speed, reaches a maximum value at V_{wind} = 4.5 m/s and V_{wind} = 6.5 m/s, and then decreases again. The cavity efficiency increases with wind speed gradually for the cases with $\beta = 45^\circ$ because the wind blow from $\beta = -45^\circ$ can not formed an "aerowindow" until the wind speed reaches 9 m/s. A higher wind speed, however, reduces the loss of hot air from the aperture and let less cold air to enter the cavity. As a result, the cavity efficiency increases with the wind speed till the "aerowindow" is formed at V_{wind} = 9 m/s [2].

10.4. The wind effect with protection of an aerowindow

In order to check the protection of the aerowindow formed by the air jet flow, cases with air jet velocity of 3 m/s, 5 m/s and 8 m/s are studied. The results are compared with the case without the aerowindow (V_{aj} = 0 m/s). Fig. 11 shows the cavity efficiency for each case. From the comparison, the cases with air jet velocity of 8 m/s have relatively higher cavity efficiency than the cases with lower air jet velocities, since a low air jet velocity may not able to form a protective curtain (aerowindow) to prevent the cold air from entering the receiver. Obviously, the cold air blown in will decrease the particle exiting temperature and the cavity efficiency by convection heat transfer [2].

For cases of no air jet flow (V_{aj} = 0 m/s), a stronger wind blowing normal to the aperture will keep more hot air in the cavity so that a higher cavity efficiency can be obtained. The case with no

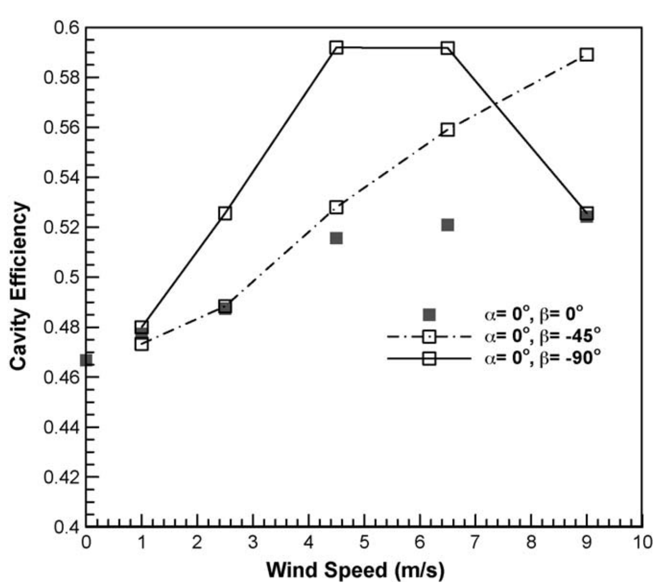


Fig. 10. The cavity efficiency for different wind speed and attacking direction (with $\alpha = 0^\circ$ and negative β).

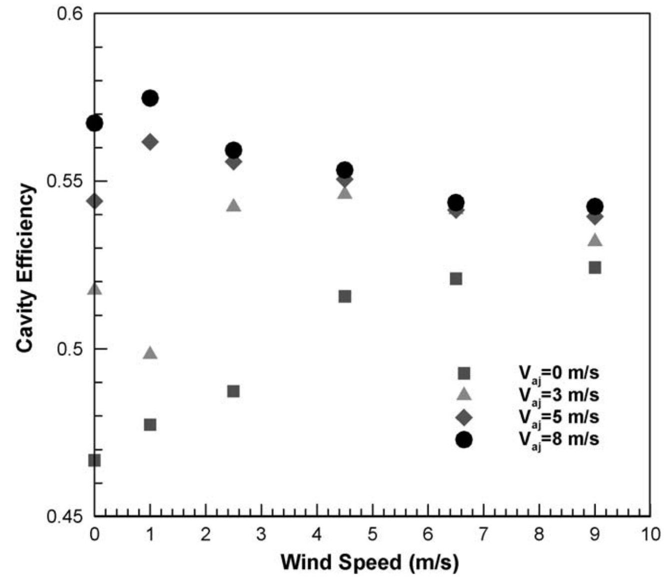


Fig. 11. The cavity efficiency for different wind speed and air jet velocity.

aerowindow and no wind undergoes a large convection loss, which causes very low cavity efficiency. For cases of air jet velocity V_{aj} = 3 m/s, the heated air in the cavity escapes quickly when there is no wind. When the wind speed increases to class one, such as 1 m/s, the blowing wind is so weak that it is unable to prevent the great convection loss by the escape of the heated air from the cavity. Moreover, the wind brings more cold air into the cavity. Therefore, the cavity efficiency decreases. When the wind speed is increased to 2.5 m/s, the stronger wind can prevent most of the escape of the heated air. As a result, the cavity efficiency increases from 50% to 54%. As can be anticipated, a higher wind speed will more efficiently keep the hot air inside the cavity. After the cavity efficiency reaches a maximum value, it will decrease again. This is because a much stronger wind will bring cold air into the cavity and decrease the efficiency after most of the hot air is kept in the cavity. For a relatively higher air jet velocity, such as 5 m/s or 8 m/s, heat loss by escape of heated air is high only when there is no wind. So, the cavity efficiency is increased when the wind velocity is increased to 1 m/s. However, when the wind speed keeps increasing, the cavity efficiency decrease again since too strong a wind speed will cause cold air to enter the cavity. Therefore, the wind effect on the performance of the solid particle receiver is very complex, especially when considering different air jet velocities. The protection of the air curtain formed by the air jet can enhance the cavity efficiency and it is better to keep the air jet injection velocity not smaller than 5 m/s. From Fig. 11, the efficiency is in the range from 46% to 57. Therefore, the cases of air jet velocity of 8 m/s will be studied as typical cases, with aerowindow comparing with the case without the aerowindow [2].

The wind attacking direction effect on the performance of a solid particle solar receiver has been studied with different wind speeds and directions. The air jet velocity is set at 8 m/s. The angle α (see Fig. 4) is first studied, while the angle β is kept to be zero. Fig. 12 shows the cavity efficiency, and Fig. 13 shows the average particle exiting temperature for all the cases. The results are compared with results from the cases with normal wind velocity ($\alpha = 0^\circ$) and results without protection of an aerowindow. The combination effect of the wind and the air jet flow is complex. Basically, the protection of the aerowindow ensures the receiver to have higher efficiency. However, the combination of the high speed wind and the air jet flow may lead to high turbulence of the air inside the cavity and cause low cavity efficiency, such as the cases with $V_{wind} \geq 4.5$ m/s and $\alpha = 45^\circ$. In an SPSR in a wind field with

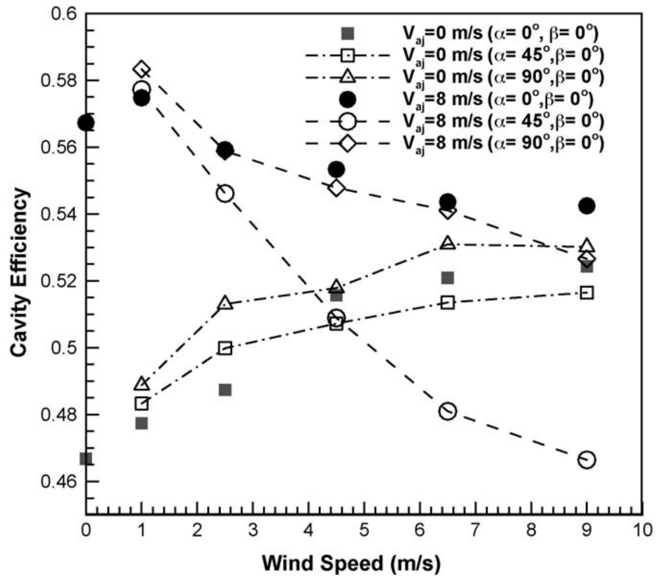


Fig. 12. The cavity efficiency for different wind speed and attacking direction.

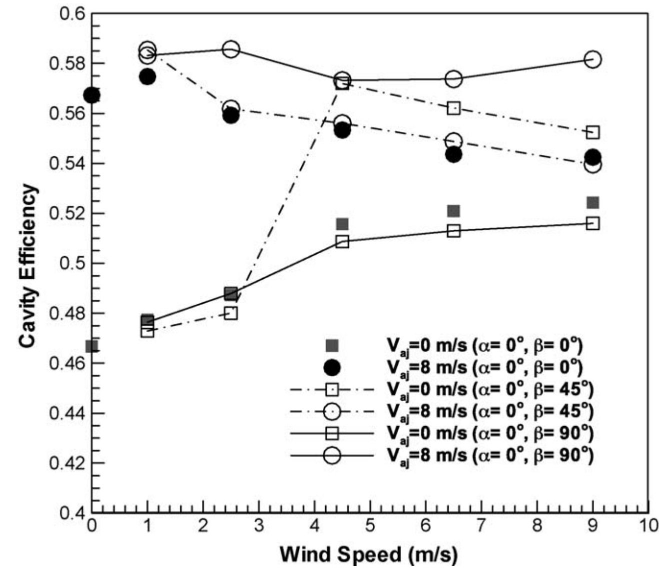


Fig. 14. The cavity efficiency for different wind speed and attacking direction (with $\alpha = 0^\circ$ and positive β).

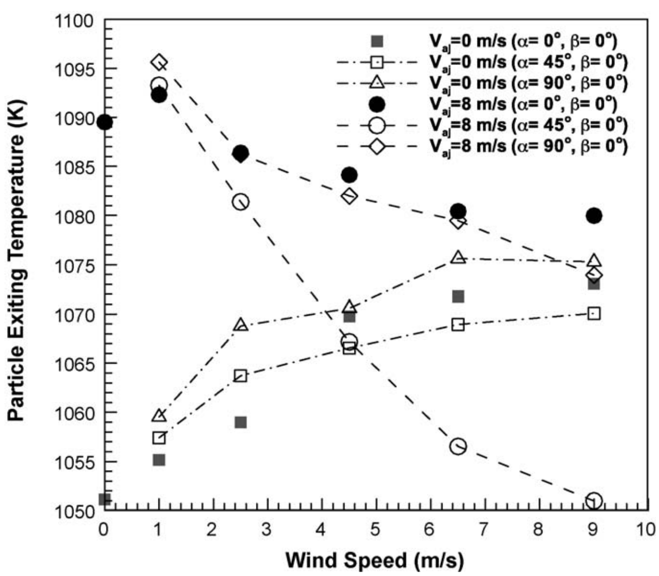


Fig. 13. The average exiting temperature for different wind speed and attacking direction.

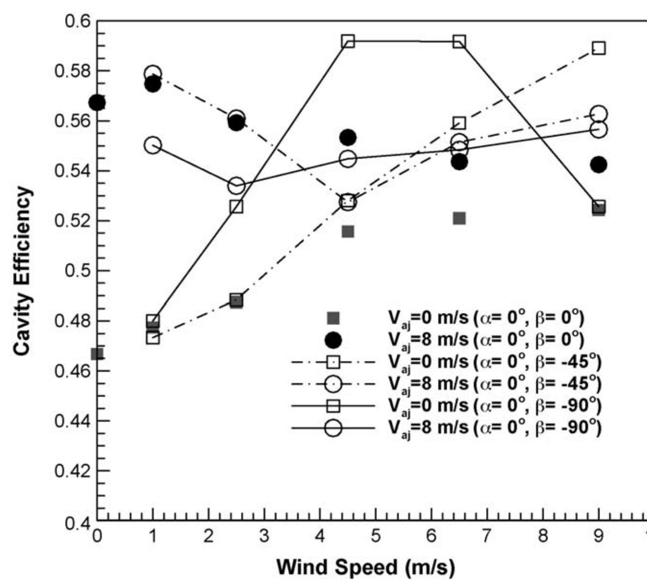


Fig. 15. The cavity efficiency for different wind speed and attacking direction (with $\alpha = 0^\circ$ and negative β).

$\alpha = 45^\circ$, the wind forces a great amount of cold air to enter the cavity from the left side of the aperture and cause a great amount of hot air to escape the cavity from the right side of the aperture. The cavity efficiency of the cases with wind attacking angle $\alpha = 90^\circ$ tends to decrease as wind speed increases, with the protection of an aerowindow formed by an air jet (V_{aj} = 8 m/s). This tendency coincides with that of the cases of $\alpha = 45^\circ$ and $\alpha = 0^\circ$ but the influence of wind on the particles is less and a higher cavity efficiency can be obtained than the cases of $\alpha = 45^\circ$.

The wind effect of different attacking angle β (see Fig. 4) is then studied, while the angle α is kept to be zero. The cavity efficiency of cases in which wind blows from the top (with positive β, typically $\beta = 90^\circ$ and $\beta = 45^\circ$) is shown in Fig. 14, compared with the cases in which the wind blows normal to the aperture. The protection of an aerowindow is very helpful for the wind blow from top (with positive β). A cavity of efficiency 54% or higher can be obtained for all the cases. For cases with $\beta = 45^\circ$ and $\beta = 90^\circ$, the air jet flow forms an ideal aerowindow easily with the help of the blowing wind. A slight decreasing of the cavity efficiency with the increasing wind speed is cased by the entrance of more cold air jet flow.

Fig. 15 shows the cavity efficiency of cases in which wind blows from the bottom (with negative β, typically $\beta = -90^\circ$ and $\beta = -45^\circ$). The wind effect is more complex if the wind blows from the bottom (with negative β). High cavity efficiency can be obtained with the protection of aerowindow a low wind speed for $\beta = -90^\circ$. When the wind speed reaches 2.5 m/s, the strong wind breaks the aerowindow from the bottom of the aperture and causes cold air to enter the cavity, and leads to a minimum cavity efficiency. When the wind speed reaches 4.5 m/s, the strong wind blowing upwards generates a circle of air at the aperture. The cavity efficiency is increased because a part of cold air enters the cavity is sucked out again. This circulation becomes strongest when V_{wind} = 9 m/s and a new aerowindow can be formed. The cavity efficiency, consequently, keeps increasing with the increasing of the wind speed from 4.5 m/s to 9 m/s.

The wind with speed of V_{wind} = 1 m/s and $\beta = -45^\circ$ presses on the air jet flow and forms an ideal aerowindow and high cavity efficiency can be obtained. When the wind speed reaches 2.5 m/s, a small amount hot air starts to escape from the cavity and the cavity efficiency starts to decrease. The cavity efficiency reaches a minimum value when the wind speed reaches 4.5 m/s because most of the air jet flow is blew away. A large amount of hot air escapes from the cavity and a large amount of cold air enters the cavity. A wind blowing from $\beta = -45^\circ$ can form an aerowindow from down side when the wind speed reaches 6.5 m/s and 9 m/s. The cavity efficiency is enhanced significantly with this reversed aerowindow [2].

10.5. The influence of the air jet temperature

The temperature of the air jet flow can be increased by a bypass heat exchanger if necessary. In order to check how this parameter affects the cavity efficiency, two cases with different air jet temperature are compared. Both cases are under the conditions of V_{aj} = 8 m/s, V_{wind} = 4.5 m/s. The basic case has an air jet temperature of T_{aj} = 300 K, and the air jet temperature for another case is enhanced to T_{aj} = 873 K. The particle exiting temperature is increased from 1084.13 K to 1087.73 K and the cavity efficiency is enhanced from 55.82% to 56.79% when the air jet temperature is increased from 300 K to 873 K. From the comparison, the increase of the air jet temperature does not enhance the cavity efficiency too much.

It was reported that the cavity of the case with T_{aj} = 873 K has a larger medium temperature region compared with the case with T_{aj} = 300 K [72]. This region with medium temperature will cause the cold air entering from the aperture be heated up earlier and one more air circulation occurs right near the exiting region of the solid particles. Besides, the air jet flow is under a high buoyancy and trying to flow up since the air jet flow has a relatively high temperature in the case with T_{aj} = 873 K. he buoyancy force hinders the formation of the aerowindow and more cold air enters the aperture, which reduces the cavity efficiency and decrease the exiting temperature of the solid particles [72].

11. Conclusions

The study on SPSRs has been reviewed, including the idea originality, the experimental work and numerical studies, and the milestones achievements. The detailed studies of a US DOE funded project on the SPSR have been reviewed. The review included the objectives of the STCH project, the conceptual design of an SPSR, the geometry, the particle properties, the calculating domain selection, the wind effect, the protection of an aerowindow and other factors which influence the cavity efficiency

A smaller size of the particles leads to a higher cavity with the same operating conditions. However, the solid particle size selection should take into account the manufacturing issues and a too small size of the particle may cause the escape of the particles from the aperture. The statistics of the wind speed and the solar incident radiation flux at a local position are analyzed. The independence of the calculating domain is studied in order to select a proper domain for the numerical simulation. In order to investigate the influences of the wind speed and wind blowing direction on the performance of the receiver, different wind conditions of and different air jet injection conditions are simulated numerically. The cavity thermal efficiencies are calculated and the optimal injection conditions are analyzed for different wind conditions. From the simulation, the influence of the wind on the performance of the SPSR is very complex. Basically, to form an aerowindow in front of the aperture of the SPSR is helpful in enhancing the cavity efficiency and the particle exiting temperature. However, the combination effect of the wind and the air jet flow may cause the efficiency to decline if the wind speed is larger than 1 m/s. The increase of the air jet temperature does not enhance the cavity efficiency too much.

Acknowledgements

This research is supported by U.S. Department of Energy, Hydrogen Program (Grant No. DE-FG36-03GO13062.).

References

[1] http://shgr.unlv.edu/v2/AboutUs/tabid/54/Default.aspx.
[2] Tan T, Chen Y, Chen Z, Siegel N, Kolb GJ. Wind effect on the performance of solid particle solar receivers with and without the protection of an aerowindow. *Solar Energy*, in press.
[3] http://www.hydrogen.gov/thepresidentshydrogen_fi.html.
[4] Koroneos C, Dompros A, Roumbas G, Moussiopoulos N. Life cycle assessment of hydrogen fuel production processes. Int J Hydrogen Energy 2004;29:1443–50.
[5] Abanades Stephane, Chsrvin P, Flamant G, Neveu P. Screening of water-splitting thermochemical cycles potentially attractive for hydrogen production by concentrated solar energy. Energy 2006;31:2805–22.
[6] Rostrup-Nielsen Thomas. Manufacture of hydrogen, *Catal Today* 2005;**106**:293–6.
[7] Deshmukh SS, Boehm RF. Review of modeling details related to renewably powered hydrogen systems. Renewable Sustainable Energy Rev 2008;12: 2301–30.
[8] Sadineni SB, Hurt R, Halford CK, Boehm RF. Theory and experimental investigation of a weir-type inclined solar still. Energy 2008;33:71–80.
[9] Beghi GE. A decade of research on thermochemical hydrogen at the joint research centre, ISPRA. Int J Hydrogen Energy 1986;11(12):761–71.
[10] Funk JE. Thermochemical hydrogen production: past and present. Int J Hydrogen Energy 2001;16:185–90.
[11] Yalc-in S. A review of nuclear hydrogen production. Int J Hydrogen Energy 1989;14(8):551–61.
[12] Brown LC, Besenbruch GE, Lentsch RD, Schultz KR, Funk JF, Pickard PS. High Efficiency Generation of Hydrogen Fuels Using Nuclear Power, GA-A24285. Prepared under the Nuclear Energy Research Initiative Program for the US Department of Energy, Dec. 2003.
[13] Kameyama H, Yoshida K. Reactor design for the UT-3 thermochemical hydrogen production process. Int J Hydrogen Energy 1981;6(6):567–75.
[14] Kameyama H, Tomino Y, Sato T, Amir R, Orihara A, Aihara M. Process simulation of 'MASCOT' plant using the UT-3 thermochemical cycle for hydrogen production. Int J Hydrogen Energy 1989;14(5):323–30.
[15] Lemort F, Lafon C, Dedryvère R, Gonbeau D. Physicochemical and thermodynamic investigation of the UT-3 hydrogen production cycle: Anewtechnological assessment. Int J Hydrogen Energy 2006;31:906–18.
[16] Bilgen C, Broggi A, Bilgen E. The solar Cristina process for hydrogen production. Sol Energy 1986;36(3):267–80.
[17] Sakurai M, Bilgen E, Tsutsumi A, Yoshida K. Adiabatic UT-3 thermochemical process for hydrogen production. Int J Hydrogen Energy 1996;21(10):865–70.
[18] Sakurai M, Miyake N, Tsutsumi A, Yoshida K. Analysis of a reaction mechanism in the UT-3 thermochemical hydrogen production cycle. Int J Hydrogen Energy 1996;21(10):871–5.
[19] Sakurai M, Bilgen E, Tsutsumi A, Yoshida K. Solar UT-3 thermochemical cycle for hydrogen production. Sol Energy 1996;57(1):51–8.
[20] O'Keefe D, Allen C, Besenbruch G, Brown L, Norman J, Sharp R. Preliminary results from bench-scale testing of a sulfuriodine thermochemical water-splitting cycle. Int J Hydrogen Energy 1982;7:381–92.
[21] Ozturk IT, Hammache A, Bilgen E. An improved process for H2SO4 decomposition step of the sulfur-iodine cycle. Energy Convers Manage 1995;36(1):11–21.
[22] Huang C, T-Raissi A. Analysis of sulfur-iodine thermochemical cycle for solar hydrogen production. Part I: decomposition of sulfuric acid. Solar Energy 2005;78(5):632–46.
[23] Kubo S, Nakajima H, Kasahara S, Higashi S, Masaki T, Abe H. A demonstration study on a close-cycle hydrogen production by the thermochemical water-splitting iodine-sulfur process. Nucl Eng Des 2004;233:347–54.
[24] Kubo S, Kasahara S, Okuda H, Terada A, Tanaka N, Inaba Y. A pilot test plan of the water-splitting iodine-sulfur process. Nucl Eng Des 2004;233:355–62.
[25] Westinghouse Electric Corporation. Solar thermal hydrogen production process, Report DOE/ET/20608-1, December; 1982.
[26] Summers WA, Gorensek MB. Nuclear hydrogen production based on the hybrid sulfur thermochemical process, Proceeding of the 2006 international congress on advances in nuclear power plants, Vol. 2006; 2006. p. 2254–2256.
[27] Steinfeld A. Solar hydrogen production via a two step water splitting cycle based on Zn/ZnO redox reactions. Int J Hydrogen Energy 2002;27:611–9.
[28] Bambergera CE, Richardson DM. Hydrogen production from water by thermochemical cycles. Cryogenics 1976;16(4):197–208.
[29] Ambriz JJ, Sibieude F, Ducarroir M. Preparation of cadmium by thermal dissociation of CdO using solar energy. Int J Hydrogen Energy 1982; 7(2):143–53.

[30] Steinfeld A. Solar hydrogen production via a two-step water-splitting thermochemical cycle based on Zn/ZnO redox reactions. Int J Hydrogen Energy 2002;27(6):611–9.

[31] Palumbo R, Lede′ J, Boutin O, Elorza Ricart E, Steinfeld A, Muller S. The production of Zn from ZnO in a hightemperature solar decomposition quench process. I—the scientific framework for the process. Chem Eng Sci 1998;53(14):2503–17.

[32] Haueter P, Moeller S, Palumbo R, Steinfeld A. The production of zinc by thermal dissociation of zinc oxide—solar chemical reactor design. Sol Energy 1999;67:161–7.

[33] Sibieude F, Ducarroir M, Tofighi A, Ambriz J. High temperature experiments with a solar furnace, The decomposition of Fe_3O_4, Mn_3O_4, CdO. Int J Hydrogen Energy 1982;7(1):79–88.

[34] Tofighi A, Sibieude F. Dissociation of magnetite in a solar furnace for hydrogen production. Tentative production evaluation of a 1000 kW concentrator from small scale (2 kW) experimental results. Int J Hydrogen Energy 1984; 9(4):293–6.

[35] Steinfeld A, Sanders S, Palumbo R. Design aspects of solar thermochemical engineering—a case study: two-step water-splitting cycle using the Fe_3O_4/FeO redox system. Sol Energy 1999;65(1):43–53.

[36] Weidenkaff A, Nuesch P, Wokaun A, Reller A. Mechanistic studies of the water-splitting reaction for producing solar hydrogen. Solid State Ionics 1997;101–103:915–22.

[37] Nakamura T. Hydrogen production from water utilizing solar heat at high temperatures. Sol Energy 1977;19:467–75.

[38] Inoue M, Hasegawa N, Uehara R, Gokon N, Kaneko H, Tamaura Y. Solar hydrogen generation with H_2O/ZnO/$MnFe_2O_4$ system. Sol Energy 2004; 76:309–15.

[39] Tamaura Y, Kojima M, Sano Y, Ueda Y, Hasegawa N, Tsuji M. Thermodynamic evaluation of water splitting by a cation excessive(Ni, Mn) ferrite. Int J Hydrogen Energy 1998;23:1185–91.

[40] Tamaura Y, Kojima N, Hasegawa N, Inoue M, Uehara R, Gokon N. Stoichiometric studies of H2 generation reaction for H_2O/Zn/Fe_3O_4 system. Int J Hydrogen Energy 2001;26:917–22.

[41] Ehrensberger K, Frei A, Kuhn P, Oswald H, Hug P. Comparative experimental investigations of the water splitting reaction with iron oxide $Fe_{1-y}O$ and iron manganese oxides $(Fe_{1-x}Mnx)_{1-y}O$. Solid State Ionics 1995;78:151–60.

[42] Tamaura Y, Steinfeld A, Kuhn P, Ehrensberger K. Production of solar hydrogen by a novel, two step, water-splitting thermochemical cycle. Energy 1995;20(4):325–30.

[43] Kaneko H, Hosokawa Y, Gokon N, Kojima N, Hasegawa N, Kitamura M. Enhancement of O_2 releasing step with Fe_2O_3 in the water splitting by $MnFe_2O_4$–Na_2CO_3 system. J Phys Chem Solids 2001;62:1341–7.

[44] Kaneko H, Ochiai Y, Shimizu K, Hosokawa Y, Gokon N, Tamaura Y. Thermodynamic study based on the phase diagram Na_2O–MnO–Fe_2O_3 system for H_2 production in three-step water splitting with Na_2CO_3/$MnFe_2O_4$/Fe_2O_3. Sol Energy 2002;72(4):377–83.

[45] Ishihara H, Hasegawa N, Aoki H, Kaneko H, Suzuki A, Tamaura Y. Two-step water splitting for solar H2 production with ZnII–MnII,III_FeIII spinel structure using concentrated solar heat. Solid States Ionics 2004;172:117–9.

[46] Kodama T, Kondoh Y, Yamamoto R, Andou H, Satou N. Thermochemical hydrogen production by a redox system of ZrO_2-supported Co(II)-ferrite. Sol Energy 2005;78(5):623–31.

[47] Pohl PI, Brown LC, Chen Y, Diver RB, Besenbruch GE, Earl BL. Evaluation of solar thermo-chemical reactions for hydrogen production. In: Proceedings of 12th Solar PACES International Symposium; 2004 6–8 Oct.

[48] Abanades S, Royere C, Flamant G. Internal PROMES-CNRS database on thermochemical cycles 2003.

[49] Charvin P, Abanades S, Flamant G, Neveu P, Lemort F. Screening and testing of promising solar thermochemical water splitting cycles for hydrogen production. WHEC 16. Lyon France; 13–16 June 2006.

[50] Kolb GJ, Diver RB, Siegel N. Central station solar hydrogen power plant. J Solar Energy Eng 2007;129(2):179–83.

[51] Hruby J, Steeper R, Evans G, Crowe C. An experimental and numerical study of flow and convective heat transfer in a freely falling curtain of particles. J Fluid Eng Trans ASME 1988;110:172–81.

[52] Hruby JM. A technical feasibility study of a solid particle solar central receiver for high temperature applications, Sandia National Laboratories, Sandia report, SAND86-8211.

[53] Meier A. A predictive CFD model for a falling particle receiver/reactor exposed to concentrated sunlight. Chem Eng Sci 1999;54:2899–905.

[54] Huang C, T-Raissi A. Analysis of sulfur-iodine thermochemical cycle for solar hydrogen production. Part I: decomposition of sulfuric acid. Solar Energy 2005;78(5):632–46.

[55] Steinfield A. Solar hydrogen production via a two step water splitting cycle based on Zn/ZnO redox reaction. Int J Hydrogen Energy 2002;27: 611–9.

[56] Steinfeld A, Imhof A, Mischler D. Experimental investigation of an atmospheric-open cyclone solar reactor for solid-gas thermochemical reactions. ASME J Solar Energy Eng 1992;114:171–4.

[57] Martin J, Vitko J. ASCUAS: a solar central receiver utilizing a solid thermal carrier, Sandia National Laboratories, SAND82-8203; 1982.

[58] Stahl KA, Griffin JW, Matson BS, Pettit RB. Optical characterization of solid-particle solar central receiver materials, Sandia National Laboratories, SAND 85-1215; 1986.

[59] Stahl KA, Griffin JV, Matson BS, Pettit RB. Optical Characterization of Solid Particle Solar Central Receiver Materials, Sandia Report SAND85-0064; 1985.

[60] Hruby JM, Burolla VP. Solid Particle Receiver Experiments: Velocity Measurements, Sandia Report SAND84-8238; 1984.

[61] Hruby JM, Steeper R, Evans GH, Crowe CT. An Experimental and Numerical Study of Flow and Convective Heat Transfer in a Freely Falling Curtain of Particles, Sandia Report No. SAND84-8714; 1986.

[62] Rightley MJ, Matthews LK, Mulholland GP. Experimental characterization of the heat transfer in a free-falling-particle receiver. Solar Energy 1992;48:363–74.

[63] Falcone PK. Technical Review of the Solid Particle Receiver Program, Sandia Report SAND84-8229; 1984.

[64] Falcone PK, Noring JE, Hruby JM. Assessment of a Solid Particle Receiver for a High Temperature Solar Central Receiver System, Sandia Report SAND85-8208; 1985.

[65] Siegel N, Kolb GJ. Design and on-sun testing of a solid particle receiver prototype. In: Proceedings of ASME 2nd International Conference on Energy Sustainability; 2008 August 10–14.

[66] Evans G, Houf W, Grief R, Crowe C. Gas-particle flow within a high temperature solar cavity receiver including radiation heat transfer. J Solar Energy Eng 1987;109:134–42.

[67] Evans G, Houf W, Grief R, Crowe C. Numerical Modeling of a SolidParticle Solar Central Receiver, Sandia Report SAND85-8249; 1985.

[68] Evans G, Houf W, Grief R, Crowe C. Gas Particle Flow Within a High Temperature Cavity Including the Effects of Thermal Radiation, Heat Transfer-Denver 1985, ASME; 1985. 81, 245.

[69] Chen H, Chen Y, Hsieh HT, Siegel N. Computational fluid dynamics modeling of gas-particle flow within a solid-particle solar receiver. ASME J Sol Energy Eng 2007;129:160–70.

[70] Siegel NP, Kolb GJ, Kim K, Rangaswamy VB. Solid Particle Receiver Flow Characterization Studies, ES2007-36118, Energy Sustainability 2007, June 27–20. Long Beach, California; 2007.

[71] Taussig Robert T, Aerowindows for Center Solar Receivers, *ASME*, 84-WA/Sol-14, p. 1–12.

[72] Tan Taide, Chen Yitung, Chen Zhuoqi. Numerical Investigation of Influences of an Aerowindow on the Performance of Solid Particle Receivers, Solar 2008-0239, May 3–8, San Diego, CA, USA.

[73] Tan T, Chen Y, Chen Z. Performance of Solid Particle Receivers with or without the Protection of an Aerowindow, ASME 2nd International Conference on Energy Sustainability, ES 2008-54129, Aug 10–14. Jacksonville, Florida, USA; 2008.

[74] Tan T, Chen Y. Performance of solid particle receivers with or without the protection of an aerowindow, *ASME J Energy Resour Technol*, in press.

[75] Fluent Inc. Fluent users guide, version 6.2.16, Lebanon, USA; 2005.

[76] Clift R, Grace JR, Weber ME. Bubbles, drops and particles. London: Academic Press; 1978.

[77] http://andvari.vedur.is/english/wind_eng.html.

[78] http://www.windows.ucar.edu/tour/link=/earth/Atmosphere/wind_-speeds.html&edu=high.

[79] U.S. Department of Energy. Data Source TMY2-23169, WMO Station 723860, Las Vegas, Nevada, U.S., http://www.eere.energy.gov/buildings/energyplus/weatherdata/4_north_and_central_america_wmo_region_4/1_usa/USA_NV_Las.Vegas_TMY2.stat.

[80] Perez-Rabago CA. Heat transfer in a conical cavity calorimeter for measuring thermal power of a point focus concentrator. Solar Energy 2006;80:1434–42.

[81] Blocken Bert. CFD evaluation of wind speed conditions in passages between parallel buildings—effect of wall-function roughness modifications for the atmospheric boundary layer flow. J Wind Eng Ind Aerodynamics 2007; 95:941–62.

[82] Fu JY. Wind effects on the world's longest spatial lattice structure: loading characteristics and numerical prediction. J Construct Steel Res 2007;63:1341–50.

[83] Bettle J. A computational study of the aerodynamic forces acting on a tractor-trailer vehicle on a bridge in cross-wind. J Wind Eng Ind Aerodynamics 2003;91:573–92.

[84] Chen Z, Chen Y, Tan T. Numerical analysis on the performance of the solid solar particle receiver with the influence of aerowindow, ASME Fluids Engineering Division Summer Conference, FEDSM 2008-55285, Aug 10–14. Jacksonville, Florida, USA; 2008.